Preprints (www.preprints.org) | NOT PEER-REVIEWED | Posted: 17 October 2018 doi:10.20944/preprints201810.0386.v1

Peer-reviewed version available at Nanomaterials 2018, 8, 896; doi:10.3390/nano8110896

Type of the Paper (Article)

Effects of residual stress distribution on Interfacial Adhesion of Magnetron Sputtered AlN and AlN/Al nanostructured coatings on (100) Silicon Substrate

Rashid Ali [1], Marco Renzelli [2], Muhammad Imran Khan [1], Marco Sebastiani [3,*] and Edoardo Bemporad [3]

[1] Faculty of Materials and Chemical Engineering, Ghulam Ishaq Khan Institute of Engineering Sciences and Technology, Topi, Swabi, KPK, Pakistan; rashidali@giki.edu.pk (R.A.); imrankhan@giki.edu.pk (M.I.K.)
[2] LFoundry s.r.l., via Pacinotti, 7 Avezzano, L'Aquila, Italy; renzelli.marco@gmail.com
[3,*] Engineering Department, Università degli studi Roma Tre, via dellaVasca Navale, 79 Rome, Italy; marco.sebastiani@uniroma3.it (M.S.); edoardo.bemporad@uniroma3.it (E.B.)
* Correspondence: marco.sebastiani@uniroma3.it ; Tel.: +39-06-57333303

Abstract: Compressive residual stresses in thin films can inhibit crack propagation under normal or sliding contact loading, with associated enhancement of the coating apparent toughness, load bearing capacity and wear resistance. This study investigates the influence of residual stress distributions on the thin film/substrate adhesion using a nanoindenter coupled with scanning electron microscope (SEM) investigations of indentation induced failure modes. Reactive and un-reactive magnetron sputtering with ion plating was used to coat a (100) silicon substrate with aluminum nitride (AlN) with and without an aluminum (Al) adhesion layer. The presence of an Al bond layer gives additional interfacial tensile stress because of the difference in thermal expansion coefficient. Additionally, a different magnitude of residual stresses in the AlN coating was achieved by changing the applied bias voltage onto the substrate. Wafer curvature method and incremental focused ion beam (FIB) milling, combined with high-resolution in situ scanning electron microscopy (SEM) imaging and full field strain analysis by digital image correlation (DIC), were used to measure the average and in-depth stress residual stress distribution in the produced coatings. The adhesion energy was then quantified by using a nanoindentation based model. Results demonstrate that the additional tensile residual stress in the aluminum adhesion layer decrease significantly the coating adhesion, even in presence of a higher compressive stress state in the AlN top-layer. Therefore, the coatings without Al-layer showed better adhesion because of a more homogeneous compressive residual stress in comparison with the coating having Al layer, even though both groups of coatings are produced under same bias voltage. Results are discussed, and some general suggestions are made on the correlation between coating/substrate property combination and the adhesion energy of multilayer stacks. The results suggested that Al bond-layer and inhomogeneous residual stresses affected the adhesion of AlN negatively to a substrate like silicon.

Keywords: physical vapor deposition; magnetron-sputtering; AlN/Al coating; silicon substrate; residual stresses; wafer curvature method; Nano-scale residual stress profiling, indentation failure modes; nanoindentation adhesion.

1. Introduction

High-quality thin coatings of aluminium nitride (AlN) has extensively been used in electronic for heat dissipation applications [1]. These coatings have been produced by several established methods. However, due to simplicity, reproducibility and lower cost, magnetron sputtering remained one of the common techniques used for the deposition of AlN coatings. One of the peculiar features of many physical vapour deposited (PVD) coatings is the presence of high compressive residual stresses [2]. These stresses are an intrinsic outcome, especially of sputtering or arc

© 2018 by the author(s). Distributed under a Creative Commons CC BY license.

Preprints (www.preprints.org) | NOT PEER-REVIEWED | Posted: 17 October 2018 doi:10.20944/preprints201810.0386.v1

Peer-reviewed version available at Nanomaterials 2018, 8, 896; doi:10.3390/nano8110896

productions, and prevents PVD-coatings to be thicker than few microns (an exception to this is electron beam made coatings those can be hundreds of microns thick, in the same range of thermal spray ones). These compressive stresses, far from being only a problem, is one of the reasons why PVD-coatings possess better mechanical resistance than coatings made with other techniques, and they are also capable of hindering nucleation and extension of cracks during service use. However, excessive compressive residual stress may result in the coating/substrate interface failure. The most advanced coating is useless if it is not well adherent to the underlying substrate and this is critical for micro-device reliability. One of the most important avenues of research for magnetron sputtered PVD-coating is to increase the adhesion of coating to the substrate under optimal residual stresses [3, 4]. However, it is much more difficult to quantify the adhesion of coatings with residual stress using nanoindentation, in respect to modulus and hardness, since the residual stress itself would affect the mechanical response of coating/substrate system.

Similar to commonly used Rockwell-C indentation (HRC) and scratch testing techniques for determining the adhesion of thick hard-coating on ductile substrate, nanoindentation is also used as enabling technique to investigate the adhesion of thin coating systems onto hard substrates. Especially in case of very thin nanostructured layers (< 1 μm), standard scratch and HRC tests fail to output reliable adhesion values, since the response of coating/substrate system becomes a strong function of substrate's properties and may change remarkably as a function of the adopted indenter tip. There are several additional benefits that make nanoindentation attractive; only small sample is needed to perform the test that can potentially supply several materials properties such as hardness, modulus and adhesion [5]. There are few studies in authors knowledge that investigate quantitatively the effect of residual stresses on contact induced coating adhesion and delamination mechanisms. A quantitative measurement of coating adhesion is essential to allow their exploitation for many critical applications, particularly within the semiconductor micro-electronics industry [6, 7]. This paper reports the work aimed to clarify the role of interfacial residual stresses on the adhesion of thin films, as measured by nanoindentation coupled with scanning electron microscopy (SEM) investigations of indentation induced failure modes.

To this purpose, two different model systems were produced: (a) a simple AlN single-layer on Si substrate, where the film was expected to be in compression; (b) the same AlN with the addition of an Aluminum relatively thick bond-layer that was designed to have a tensile residual stress in the Aluminum layer (as it usually happens for Al metallic PVD layers).

In this way, the effects of an inhomogeneous state of stress (tensile-compressive) on adhesion of the coatings was assessed.

Finally, the same AlN (with and without an Al bond layer) coatings were also deposited under higher bias voltage conditions, in order to investigate the effects of an increased compressive stress in the top-layer on adhesion.

By combining the results from the four different samples, a discussion was made on how the residual stress distribution in Al/AlN PVD coatings would affect adhesion and crack propagation modes.

2. Experimental Details

Coating were produced using a PVD sputtering plant, with direct current (DC) powered aluminium targets and radio frequency (RF) powered capacitive coupled sample holder capable of inducing bias to conductive and dielectric substrates. Nitrogen was put into the chamber to produce aluminium nitride by reactive sputtering. The Aluminium nitride thin films were deposited on ≈ 290 μm thick rectangular single crystal (100) silicon wafers (20 x 7 mm^2), with an initial average roughness (Ra) of ≈ 10 nm. Prior to sputtering, silicon substrates were cleaned with acetone and ethanol for five minutes in each. Samples were mounted on a sample holder that was placed at a distance of 80 mm from the target. These substrates were subsequently sputter-etched in argon plasma for 10 min in order to remove the surface oxide layer. Four samples were deposited with an AlN coating using 180 W DC on the 200 mm Al cathode, a gas mixture of 25 % argon and 75 % nitrogen, process pressure of 1×10^{-4} mbar and a base pressure lower than 6×10^{-6} mbar. With these deposition parameters, the

Preprints (www.preprints.org) | NOT PEER-REVIEWED | Posted: 17 October 2018 doi:10.20944/preprints201810.0386.v1

Peer-reviewed version available at Nanomaterials 2018, 8, 896; doi:10.3390/nano8110896

cathode was fully poisoned, ensuring a perfect stoichiometry of the produced coatings; the low power density on the aluminium targets ensured no arcing and thus no particle production. The four samples differed for the applied negative bias voltage to the substrate during growth and the optional presence of 50 nm thin pure aluminium bond layer; the samples with or without bond layer were coated with an applied floating potential (around 30 V from the plasma) or 100 V RF applied potential. The maximum temperature developed during deposition and ion-etching was measured with a temperature measurement strip gauge. These strip gauges were mounted onto the aluminum sample holder which held the sample on other side. At the end of deposition, maximum temperature of ≈ 150 °C was recorded. To facilitate reading, the produced coatings were investigated by dividing into two groups, one without bond-layer under floating bias of 30 V and bias voltage of 100 V; named as AlN-30V and AlN-100V, respectively. In the second group, AlN coating under bias voltage of 30 V and 100 V with aluminium bond layer; named as AlN/Al-30V and AlN/Al-100V, respectively.

After deposition, the wafer curvature method (extended Stoney formula) was used for average residual stress measurement in which bi-axial state of stress was taken into consideration [8, 9]. The choice of (100) silicon, and its more complex stiffness in respect (111) silicon was due to the need to have perfectly rectangular strips (111 silicon tends to cleavage in triangles). Curvature profiles were measured on the coating side. As widely known from literature, a concave surface curvature corresponds to compressive residual stress in the characterized coatings. Curvature was then measured using state of the art optical profilometer (Leica DCM-3D) in accordance with standard procedure CEN/TS 1071-1 [10]. Optical profilometer enables accurate and reproducible curvature measurements with z-height resolution of ≈ 0.6 nm. A 2-D coating surface profile up to 8 mm scan length was constructed with extended topography in confocal mode. Radius of curvature was measured through circle fitting of 2-D profile and residual stresses were calculated by the modified Stoney equation:

$$\sigma = M_{(100)} \frac{t_s^2}{6t_c} \frac{1}{R} \quad (1)$$

Where, ts and tc are the thickness of substrate and coating, respectively, and M (100) = $\frac{E_S}{1-\vartheta_S}$ is the bi-axial modulus of single-crystal silicon (100) which is 180.4 GPa [11]. Thickness of coating was measured with optical profilometer (step height method) and verified with focused ion beam (FIB) FEI Helios NanoLab 600 Dualbeam FIB/SEM cross-section analysis.

The through-thickness gradient of residual stress was measured by using a novel incremental micro-ring core method [12-14], which consists of controlled material removal by focused ion beam (FIB) microscopy, coupled with SEM high-resolution imaging, digital image correlation (DIC) for relaxation strain analysis, and finite-element (FEM) calculation of the residual stress depth gradient. As described in a recent paper, this new method allows for nano-scale depth profiling [14] of the residual stress in thin films. In this paper, this method was applied to the coatings with Al interlayer (both deposited at -30 and -100 V bias voltage)in order to investigate the residual stress gradient in proximity of the AlN/Al interface. The same method, also allow for the estimation of the average residual stress in the film, and a comparison with results from curvature analysis was made.

The elastic-modulus and hardness of coatings were measured by nanoindentation testing in accordance with ISO 14577 standard (Keysight G200 Nano Indenter®, 0.05 s^{-1} constant strain rate, maximum indentation depth 1000 nm), by employing the Continuous Stiffness Method (CSM), which allows to calculate the hardness (H) and elastic-modulus (E) profiles versus penetration depth (it is the superposition of a oscillatory varying load to the linearly increment in indenter depth). For all nanoindentation experiments, the frame compliance and indenter tip area function was calibrated on standard fused silica block and following the procedure suggested by Oliver and Pharr [15]. As the coating had a thickness in the order of ≈ 700 nm, the most reliable values of hardness and modulus were obtained by interpolation of the CSM hardness/modulus versus depth profiles and the calculation of the interpolated average H and E values in the depth range of 60-70 nm. In this way, the effects coming from substrate's influences are reduced (this is especially true for hardness, while the elastic modulus is always influenced by the substrate compliance).

Preprints (www.preprints.org) | NOT PEER-REVIEWED | Posted: 17 October 2018 doi:10.20944/preprints201810.0386.v1

Peer-reviewed version available at Nanomaterials 2018, 8, 896; doi:10.3390/nano8110896

Adhesion of coatings was assessed by equipping the nano-indenter with a cube-corner tip and making load-controlled indentation in order to induce coating delamination, using a maximum load of 200 mN. Nine indents on each sample were made and at least five indents were observed by scanning electron microscope (SEM). The interface adhesion of coatings under different residual stress conditions were evaluated using the den-Toonder et. al model [16], through microscale observation of indentation induced failures. Originally, Thouless [17] proposed this model for interfacial adhesion through observation of triangular coating spallation failure with scratch tests. Later, den-Toonder et.al [16] modified this model to take into account the curved geometry of the delaminated segment and residual stresses, which is usually produced failure in residual stressed coating under nanoindentation. In this work, this model was used to quantify interfacial adhesion of the films.

3. Results and Discussion

3.1. Residual Stress Measurement

An isometric view of typical 2-D profile of silicon wafer curvature measured with optical profilometer is shown in the Figure 1 while curvatures for other samples are not shown here for simplicity.

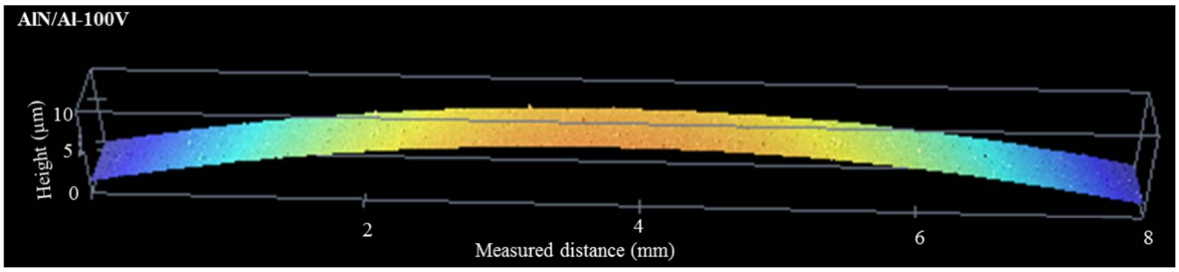

Figure 1. Example of optical profilometer measured radius of curvature of the coatings after deposition.

Coating thickness and microstructure was analyzed with FIB-TEM section analysis (Figure 2), while residual stress was calculated using the curvature method, as reported in Table 1. As clearly visible in figures 2, the presence of an Al bond layer does not change at al the microstructure of the AlN layers, which are made of very fine columnar nanostructured grains.

Table 1. Description of coatings deposition parameters, measured overall coating thickness and compressive residual stress with wafer curvature method.

Description of coatings	Bias Voltage (-V)	Bond-layer (Yes/No)	Thickness (µm)	Average Residual Stress (Curvature - GPa)
AlN-30V	30	No	0.75 ± 0.05	-1.2 ± 0.2
AlN/Al-30V	30	Yes	0.76 ± 0.02	-1.5 ± 0.2
AlN-100V	100	No	0.72 ± 0.03	-3.5 ± 0.2
AlN/Al-100V	100	Yes	0.71 ± 0.04	-3.9 ± 0.2

The average residual stress values are shown in Figure 3, as calculated by Stoney and FIB-DIC methods. For the two samples where two techniques are used, there is good agreement between the data (i.e. the discrepancy is within the standard deviations), as also reported in previous literature.

On comparing the coating in first and second group, significantly higher residual stress was found under polarization of the substrate with negative potential of 100V (AlN-100V coatings), compared to substrate under polarization of 30V (AlN-30V coating). This is an expected result, and the increase of average compressive residual stress for all coatings that were deposited at -100V bias

Preprints (www.preprints.org) | NOT PEER-REVIEWED | Posted: 17 October 2018 doi:10.20944/preprints201810.0386.v1

Peer-reviewed version available at Nanomaterials 2018, 8, 896; doi:10.3390/nano8110896

voltage can be attributed to an atom peening effect given by the increased energy of the vapor flux. In case of the AlN coatings on Silicon, the thermal component of the residual stress can be considered as negligible with respect to the atomic peening component, since the thermal expansion coefficients of the two materials (AlN and Silicon) are similar.

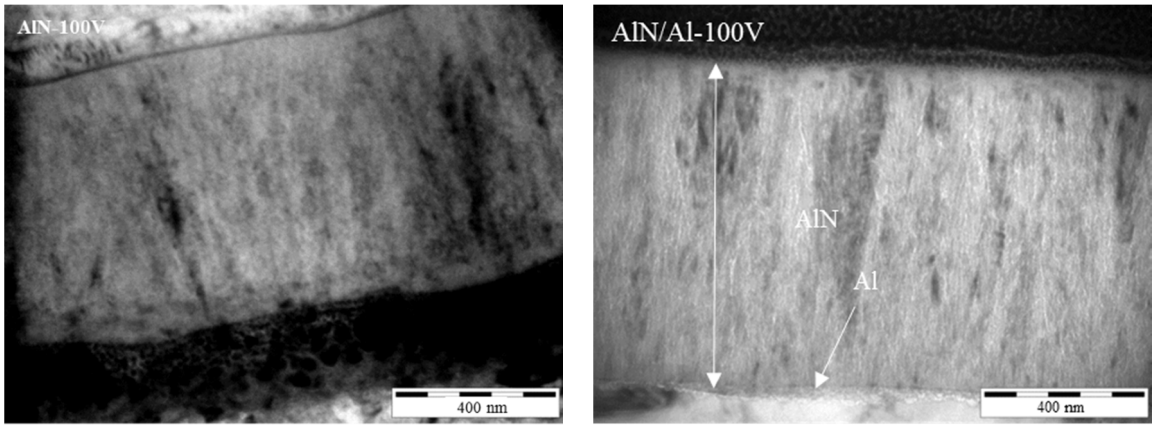

(a) (b)

Figure 2. TEM observations (after Focused ion beam cross-sections) of produced coating for coating thickness measurement: **(a)** AlN-100V; **(b)** AlN/Al-100V.

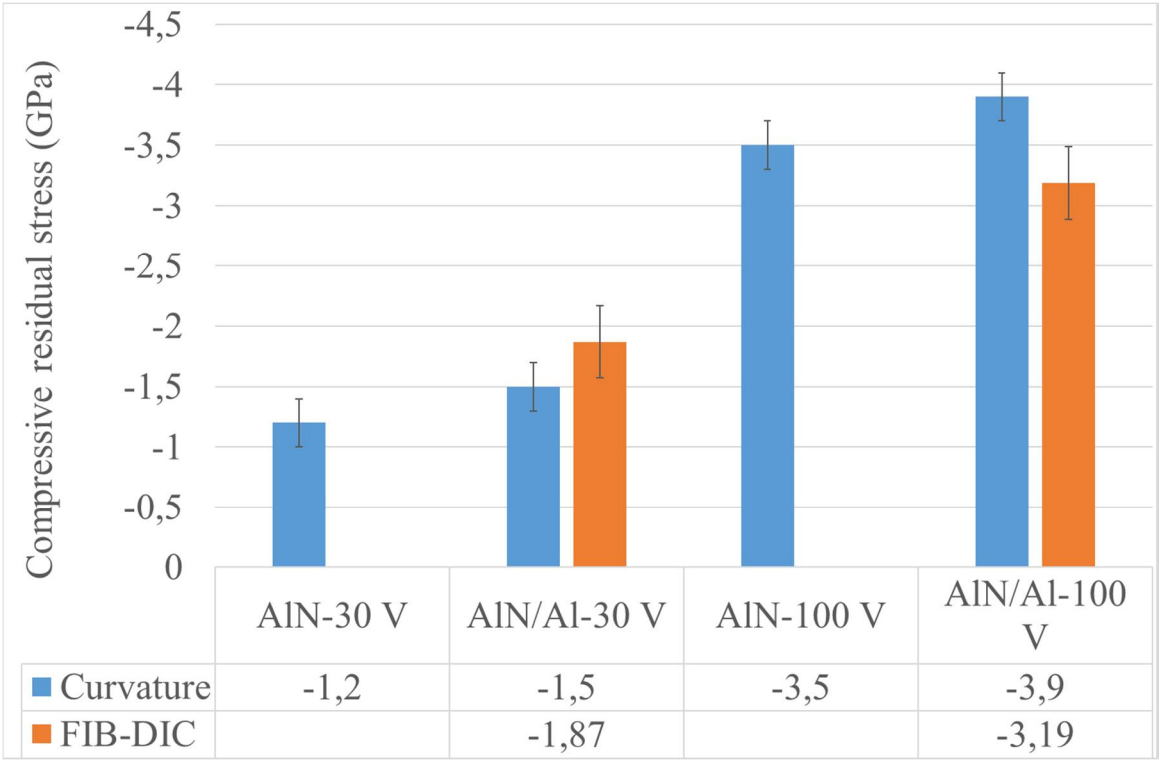

Figure 3. Plot of average compressive residual stress (curvature measurements) and FIB-DIC in all the produced coatings.

On the other hand, in AlN coating with Al bond-layer the thermal stresses component has contributed significantly to an increase in overall residual stresses in AlN/Al coating system as shown in the figure 3 (under the assumption that the atomic peening component remains the same). Castanho et.al [18] observed a similar phenomenon in magnetron sputtered multi-layer coatings, whereas the number of aluminum interlayers was increased, more compressive stresses were induced in the top-layer of AlTiN. In fact, the contribution of thermal stresses was analytically evaluated to be ≈ +340 MPa by using the thermal expansion of substrate (Si, 2.3 x 10^{-6} $°C^{-1}$) and bond layer (Al, 22.8 x 10^{-6} $°C^{-1}$) reported in literature [7]. The aluminum bond layer during cooling from the

Preprints (www.preprints.org) | NOT PEER-REVIEWED | Posted: 17 October 2018 doi:10.20944/preprints201810.0386.v1

Peer-reviewed version available at Nanomaterials 2018, 8, 896; doi:10.3390/nano8110896

deposition temperature attempted to contract more than the silicon substrate and AlN coating. However, at interfaces, the aluminum cannot contract fully due to the constraining by the silicon substrate and AlN top-layer, and as a result the aluminum bond layer is in tension, which cause additional compression residual stresses in the AlN coating and silicon substrate. By considering these thermal stresses contribution into account, the residual stress variation between coatings with and without bond layer reported in figure 3 is largely explained.

Furthermore, the FIB-DIC analysis of residual stress depth-profile in the AlN layers is a further confirmation of the above discussions. In fact, in both cases (AlN/Al with -30V and -100V bias) we do observe a strong surface compressive residual stress that goes towards tensile when approaching to the AlN/Al interface. In case of the AlN/Al-100V system, we even observed a mild state of tensile stress in the AlN layer in the vicinity of the interface. For this sample, the presence of a tensile stress approaching the interface is a further explanation for the extensive delamination that were observed during the indentation.

Therefore, the adoption of an additional Al interlayer, in this specific case, give rise to an increased compressive stress in the top layer (AlN) and (at the same time) a stronger stress gradient and an additional tensile residual stress at the interface (figure 4c).

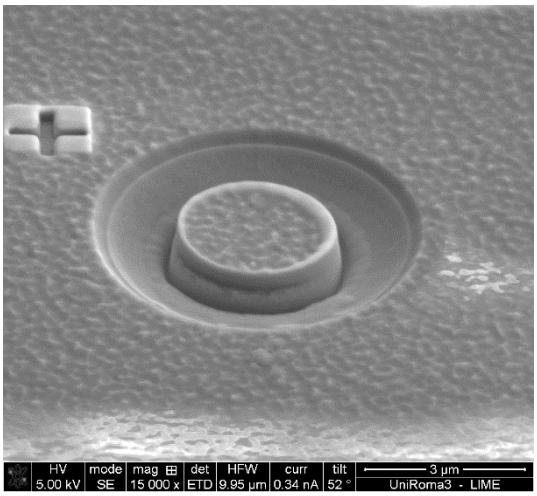

(a)

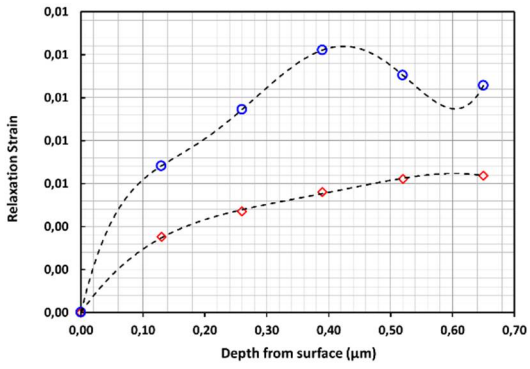

(b)

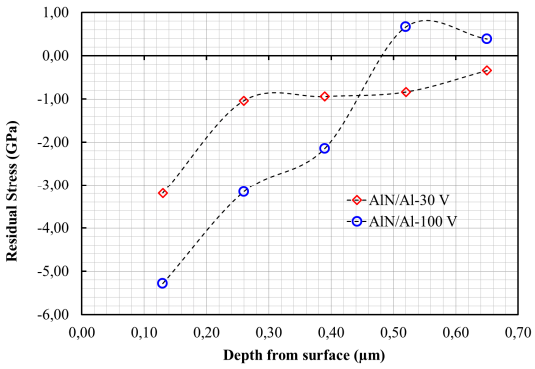

(c)

Figure 4. Results of FIB-DIC residual stress characterizations. (a) example of micro ring-core test; (b) Representative relaxation strains vs milling depth for the two coatings with Al bond layer; (c) Representative residual stress profiles for the two coatings with Al bond layer (AlN/Al with -30V and -100V bias), obtained by using the FIB-DIC depth profiling method described in [14].

Preprints (www.preprints.org) | NOT PEER-REVIEWED | Posted: 17 October 2018 doi:10.20944/preprints201810.0386.v1

Peer-reviewed version available at Nanomaterials 2018, 8, 896; doi:10.3390/nano8110896

3.2. Nanoindentation Characterizations

3.2.1 Hardness and Elastic Modulus

Hardness and elastic modulus of all the produced coatings were measured with the Berkovich indenter and results are summarized in Figure 4.

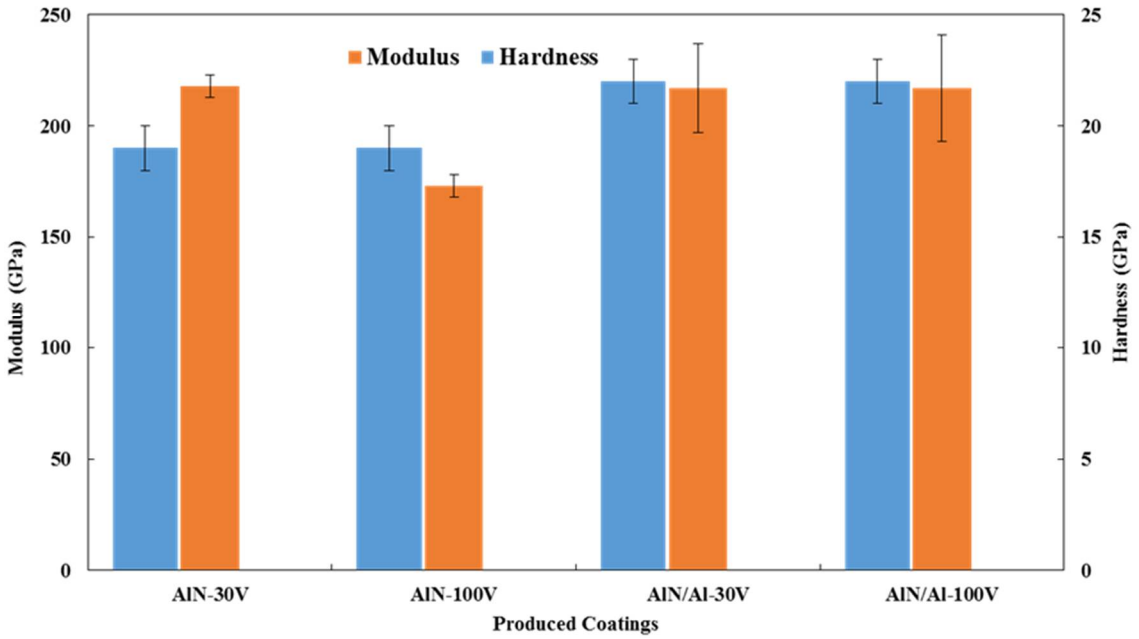

Figure 4. Results of nano-indentation hardness and elastic modulus.

There is a minor difference in the measurement between AlN coatings with and without bond layer. Coatings made with bond layer have higher standard deviation that those without it. The major source of deviation in nanoindentation hardness and modulus is roughness of the coating surface, and it is possible to see in Figure 5 show the surface of the coating AlN-30V and AlN/Al-30V are different.

The nanoindentation results further demonstrate that the only (and main) difference among the coatings is the residual stress and its distribution. Therefore, the main difference in adhesion could only be attributed to the different residual stress distribution.

The subsequent sections summarize the results of coating/substrate interfacial adhesion, failure modes and their effect analysis.

3.2.2. Quantitative Evaluation of Coating Interfacial Adhesion

The interfacial adhesion energy of coatings was investigated by analyzing micro-scale delaminations failures produced under Berkovich and cube-corner indenter tips. At first, nanoindentations have been made with standard Berkovich indentation tip. Figure 5 shows the load-displacement curves and the associated SEM micrograph of an indent in the four cases under consideration.

As clearly visible from this figure, the coating/substrate adhesion decreases dramatically for the two coatings with an Al layer.

The discontinuous cracks formed in the indents of coating AlN-30V and AlN-100V (as indicated by picture-frame cracks shown in Figure 5) seems due to tensile stresses induced by the dragging of the part of coating around indenter from the bulk of coatings. An extensive analysis of this kind of cracks is reported in [19], where it is explained that they are related to the ratio mismatch E/H between coating and substrate. The discontinuity in displacements during the unloading segment is related to reverse phase transformation in the silicon substrate [20, 21].

Preprints (www.preprints.org) | NOT PEER-REVIEWED | Posted: 17 October 2018 doi:10.20944/preprints201810.0386.v1

Peer-reviewed version available at Nanomaterials 2018, 8, 896; doi:10.3390/nano8110896

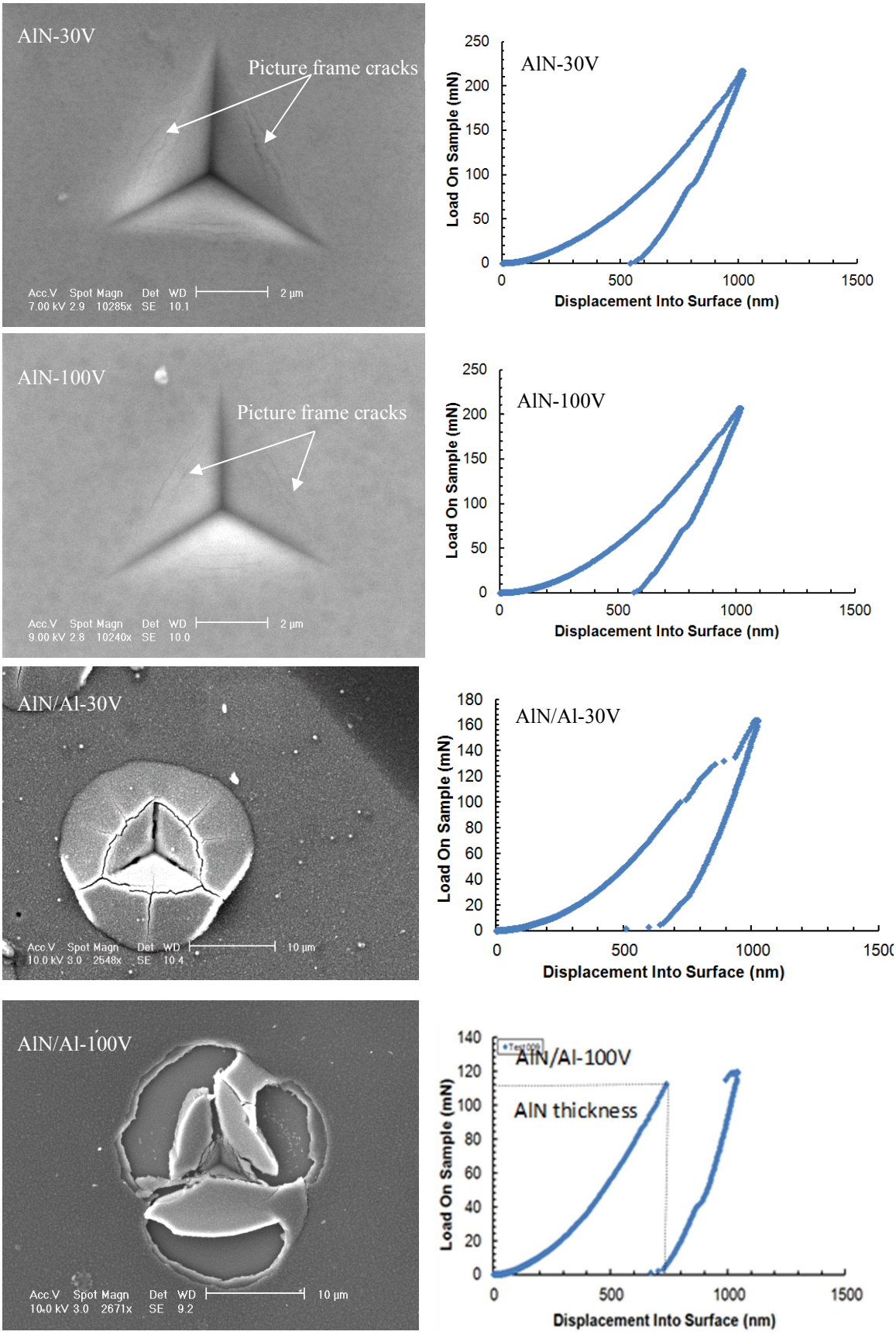

Figure 5. The SEM micrographs of indentation (in left column) made with the Berkovich indenter and associated load-displacement curves (in right column).

Preprints (www.preprints.org) | NOT PEER-REVIEWED | Posted: 17 October 2018 doi:10.20944/preprints201810.0386.v1

Peer-reviewed version available at Nanomaterials 2018, 8, 896; doi:10.3390/nano8110896

Only the coatings with Al bond layer, AlN/Al-30V and AlN/Al-100V presented extensive buckling and delamination with the Berkovich indenter at 140 mN and 120 mN indentation load, respectively, as shown in right column of Figure 5. The load-displacement curve in coating (AlN/Al-100V) at thickness of ≈ 750 nm exhibited a displacement burst (horizontal step) and confirms the through-thickness cracking leading to interfacial detachment of the coating. The metallic film (bond layer) is likely to undergo plastic deformation and these deformation could be significantly larger than film thickness [22]. From these observations, it was clear that coating (AlN/Al-100V) has poorest adhesion as it delaminated completely at lower load and it also has higher residual stress in comparison with AlN/Al-30V coatings.

After these tests, all the four coatings were tested again with a cube corner indenter, for producing fracture. The coatings (AlN-30V and AlN-100V) without bond layer did not delaminate up to the substrate (Figure 6), but only showed cracks within the film thickness.

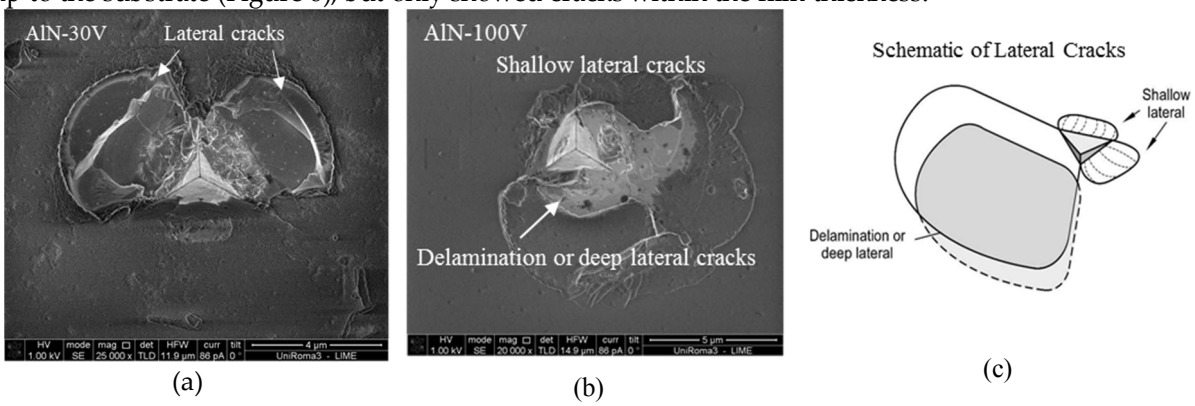

Figure 6. The SEM micrographs of indentation made with cube-corner indenter: **(a)** coatings AlN-30V; **(b)** AlN-100V (at different magnifications); **(c)** Schematic of lateral cracks [23].

The SEM indentation micrograph of coatings (AlN-30V and AlN-100V) clearly shows that central region is shallow to various depths compared to mean level of the coating (Figure 6) and cracks morphology is similar to usually observed lateral cracks. The propagation of crack through formation of steps followed by turning upward to form chips is confirmation of lateral cracks and crack propagation is similar in the two coatings micrographs. It is possible that higher residual stress magnitude caused the chipping (possible delamination) failure seemingly due to weaker adhesion in AlN-100V coatings. However, the coatings AlN-30V having good adhesion, indenter cause lateral cracks without delamination. The possibility of change in crack pattern with sharp cube-corner indenter are expected as a result of substrate effect.

For this lateral cracking in coatings (AlN-30V and AlN-100V), a fracture toughness value of 1.8 and 2.3 MPa $m^{0.5}$ was estimated with den-Toonder model (Equation 1) [16] which originally developed by Antis et.al [24] to investigate the fracture toughness of bulk materials. The input of this model are the crack load (80 and 100 mN for the coatings AlN-30V and AlN-100V respectively), the length of lateral cracks, crack depth which is equal to half of coating thickness and the measured residual stresses in the coatings. It has to be underlined that such values should be only considered as rough estimation of coatings' fracture toughness, since there are many factors affecting the reliability of such indentation-based methods, as discussed in recent papers [25]. Nonetheless, the estimated fracture toughness of coatings are very similar and in the range of the toughness (1.5 - 5 $MPa.m^{0.5}$) of ceramic coatings reported in the literature. This estimation has an error of 0.2 MPa $m^{0.5}$ (normally the error is much higher for this kind of measures, around 30%); this low error values comes from the repeatability of results. It was expected that higher stresses under higher bias voltage were to be correlated with higher toughness of coating, but this is not the case. The measurements show that the higher load to crack of the coating AlN-100V is due to the compressive intrinsic stresses, and once this effect is taken into account, there are no major toughness difference between two coatings.

Preprints (www.preprints.org) | NOT PEER-REVIEWED | Posted: 17 October 2018 doi:10.20944/preprints201810.0386.v1

Peer-reviewed version available at Nanomaterials 2018, 8, 896; doi:10.3390/nano8110896

For the coatings with Al bond layer, the cube corner indenter achieved full coatings delamination from the substrate, and the den-Toonder Model [16] can be used to quantify interfacial adhesion energy. According to this model, indenter has only the role of crack initiator, and residual stresses are the driving force for delamination and chipping. The input of this model are the measured coating thickness, elastic modulus, residual stresses and chipped coating segment geometric information as elaborated in Figure 7c.

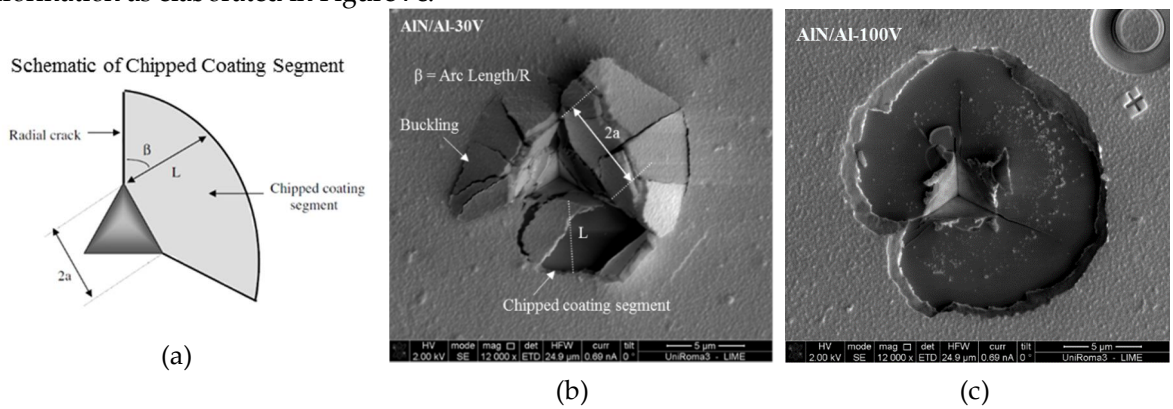

(a) (b) (c)

Figure 7. (a) Schematics of chipped coating segment [16]; **(b)** The SEM micrographs of indentation induced failures for adhesion measurement of AlN/Al-30V; **(c)** The SEM micrographs of indentation induced failures AlN/Al-100V coatings.

Coatings segment formed chips can be clearly seen in the micrograph of coatings (AlN/Al-30V) which is semi-circle with an easily identifiable radius and chipped region has similar schematics for which den-Toonder developed the model (Figure 7). Comparison of micro-scale delamination failures mode (semicircular) in Figure 7, it is also possible to see that large circular chipping in coating (AlN/Al-100V) is higher than the ones in AlN/Al-30V coatings. The coatings (AlN/Al-30V) having lower residual stresses in comparison with coating (AlN/Al-100V) having higher residual stresses showed different delamination failure, however, the mode of delamination in almost all of the indents were circular (Figure 8).

The den Toonder et.al model [16] (Equation 10) resulted in interfacial adhesion energy of 5 and 4 J/m^2 for the coatings (AlN/Al-30V and AlN/Al-100V), respectively. The estimations have an error of ± 5 %. The calculated adhesion energy is practical interfacial fracture energy and it also includes the elastic strain energy associated with the release of residual stresses. The interfacial fracture energy or the adhesion energy results are in accordance with the qualitative comparison of indentation-induced failures produced with the cube-corner indenter. In addition, adhesive failure modes of coatings (AlN/Al-30V and AlN/Al-100V) are compared with literature which are in good agreement with those given by Bull [26]. The results indicates that adhesion of coating has been deteriorated, in this specific case, due to the presence of the aluminum bond layer. As the coatings (AlN-30V and AlN/Al-30V) have difference in compressive residual stress of only +340 MPa, we can expect that the Al bond layer is in tensile stress state by a similar magnitude.

This assumption can be justified by thinking to the additive nature of residual strains in multilayer systems. The bond layer being ductile cannot store elastic energy across the interface and tensile residual stresses are also present in it (as also observed by FIB-DIC stress profiles). The tension coupled with deformation during indentation in Al bond layer leads to interfacial delamination. In most of the studies available in literature, AlN was directly coated onto silicon substrate; nonetheless, there are few studies that use thin layer of Al to improve bonding between AlN and Si substrate even though adhesion was not investigated [27].

Preprints (www.preprints.org) | NOT PEER-REVIEWED | Posted: 17 October 2018 doi:10.20944/preprints201810.0386.v1

Peer-reviewed version available at Nanomaterials 2018, 8, 896; doi:10.3390/nano8110896

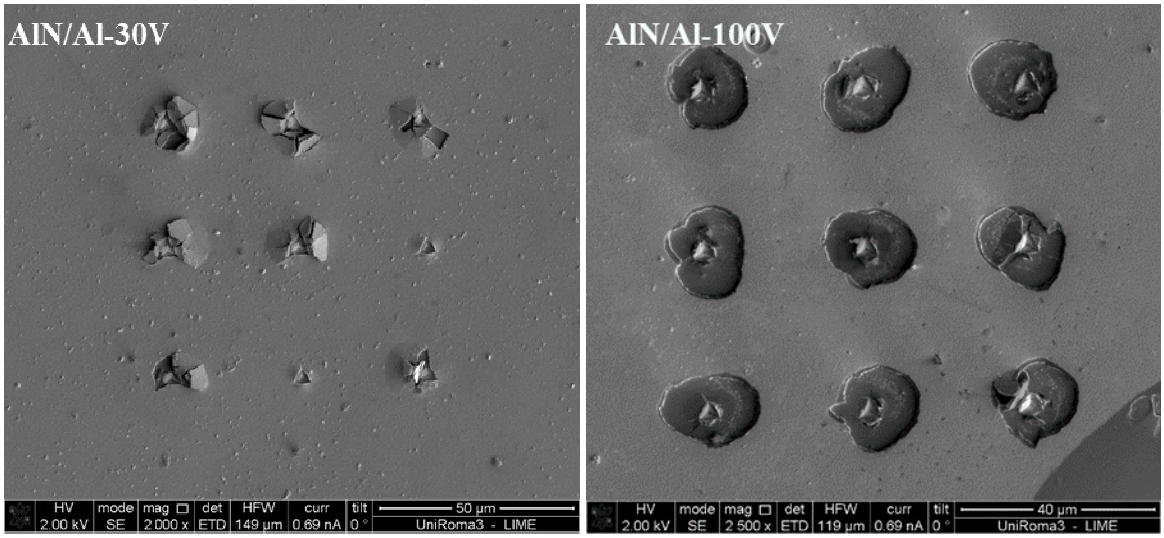

(a) (b)

Figure 8. The SEM micrographs of indentation induced failure of all the indents made for adhesion measurement in: **(a)** AlN/Al-30V; **(b)** AlN/Al-100V coatings.

In this work, we have shown that the role of the residual stress in the bond layer is significant, because even only ≈ 50 nm thin layer is capable to break by bulging the ≈ 700 nm thick upper layer, decreasing the functional adhesion of coating under nanoindentation (Figure 8). Therefore, we demonstrate here that the residual stress state in the Al bond layer can have a primary and relevant effect on coating's adhesion, more than the residual stress and hardness of the AlN top layer.

Also, bond layer being ductile, one would expect an increase of the interfacial adhesion energy because of decrease of stored elastic energy across the interface. However, as indentation depth exceeds the top layer thickness (AlN), a step in load-displacement curve occurs (right column of Figure 5) in coating AlN/Al-30V and AlN/Al-100V. As a result, the soft bond layer, like pure aluminum and copper, is not up to the task to be a proper coating base, especially if the substrate is hard. This is the reason why only bond layers made of Ti, Cr, Mo or Nb are effective on to the hard substrate for smooth transition of properties between hard coating and substrate [28, 29]. Comparison of coating delamination behavior under different residual stress conditions suggested (Figure 8) that both the mode I and mode II load components in the buckled and unbuckled states are operative. The schematic of both the buckled and unbuckled failure modes are given in Figure 9 for reference.

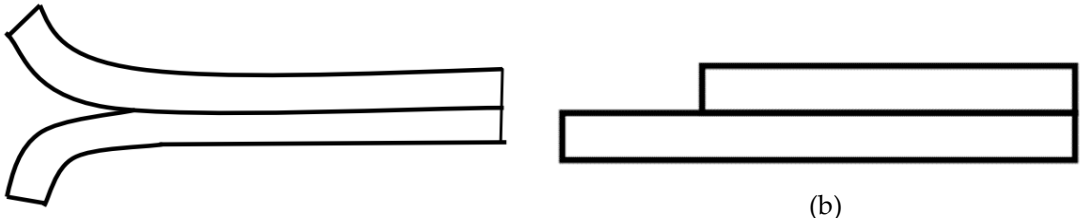

(a) (b)

Figure 9. Schematic of interfacial crack initiation modes: **(a)** mode I failure; **(b)** mode II failure [30].

It can be seen in micrograph of Figure 8b that coatings (AlN/Al-100V) shows shear mode II and failure can be characterized as catastrophic with highest delamination, however, in coating (AlN/Al-30V) a mixture of peeling (mode I) and shear (mode II) delamination failures were observed as a result of tensile stress in aluminum coating layer and compressive stresses in AlN layer. It is possible that at about critical indenter penetration, the higher compressive stresses of indentation resulted buckling in soft thin film of aluminum, which means that interfacial adhesion is not too high. The buckling failure is more likely than the shear-induced delamination when the coating is relatively tough compared to the interface. In order to confirm, whether the coating delaminates from AlN/

Preprints (www.preprints.org) | NOT PEER-REVIEWED | Posted: 17 October 2018 doi:10.20944/preprints201810.0386.v1

Peer-reviewed version available at Nanomaterials 2018, 8, 896; doi:10.3390/nano8110896

bond layer interface or from bond layer/substrate interface, energy dispersive spectroscopy (EDS) composition maps were performed (Figure. 10).

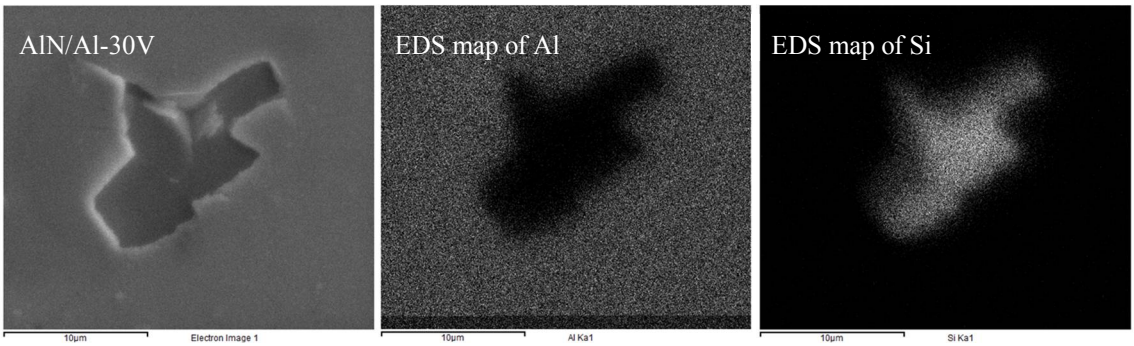

(a)

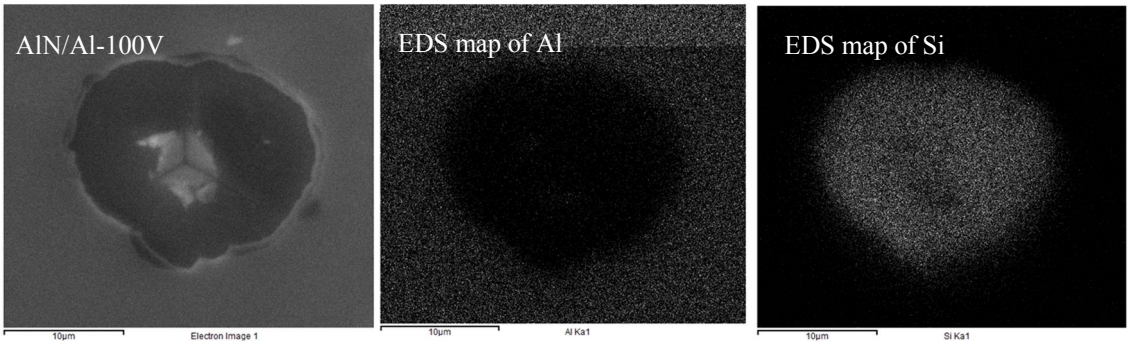

(b)

Figure 10. The EDS maps of cube-corner produced indentation marks in coatings and corresponding mapping images of Al and Si elements: **(a)** AlN/Al-30V; **(b)** AlN/Al-100V.

The EDS map of aluminum in second column of Figure 10 shows that aluminum is present in the AlN layer, however, it is not present where coatings has been delaminated. Similarly, silicon EDS map in the third column from left shows that silicon is not present in AlN coating and silicon substrate is exposed after delamination. It is noticeable that silicon substrate is visible and bond layer is missing in the EDS map even though bond layer thickness was measured and confirmed with FIB-TEM cross-section analysis (shown and indicated in Figure 2). This shows that delamination failures are from the bond layer and substrate interface while bonding between AlN and Al is perfect. The results indicate that adhesion of coating has been deteriorated due to aluminum bond layer and the surface fracture is the interface between aluminum and silicon. Using this information and the measured interfacial delamination energy (G_{int}) of 5 and 4 J/m^2 for the coatings (AlN/Al-30V and AlN/Al-100V), respectively; the interface fracture toughness (K_{int}) defined by Suo and Hutchinson [31] may be estimated using Equation 2.

$$K_{int} = \sqrt{G_{int} E_{int}} \quad (2)$$

Where, Eint is interface elastic modulus and is given by Equation 3.

$$\frac{1}{E_{int}} = \frac{1}{2}\left[\frac{1}{E} + \frac{1}{E_s}\right] \quad (3$$

Using E as coating modulus and Es as substrate modulus, the interface elastic modulus (Eint) was found to be 100 GPa. The estimated interface fracture toughness of 0.71 and 0.65 MPa m$^{0.5}$ for the coatings (AlN/Al-30V and AlN/Al-100V) clearly indicate why these coatings delaminated instead of cracking as the resulting interfacial fracture toughness is significantly lower than the cohesive fracture toughness of coatings (AlN-30V and AlN-100V).

The technological implications of this study results for the design and production of coatings on hard substrate and, in particular, on the silicon substrates for various applications. For example,

Preprints (www.preprints.org) | NOT PEER-REVIEWED | Posted: 17 October 2018 doi:10.20944/preprints201810.0386.v1

Peer-reviewed version available at Nanomaterials 2018, 8, 896; doi:10.3390/nano8110896

aluminum nitride and other ceramic coatings are of industrial interest as a next generation material for sensor applications. Ionescu et.al. [32] indicated the real possibilities of manufacturing sensors embedded on the monitored components of machine tools [33]. The strength of silicon wafer used in solar cell and micro-electronics applications could be improved with hard-coatings [34]. Also, the micro-scale produced failure modes and their effect analysis is addition to contact induced coating failures which could help to validate the coating adhesion models. In all that, the experimental characterization adds new information to literature that may help to interpret the contact induced failures in coatings under tribological situations, by focusing in particular on the role of the residual stress distributions for the case of metal/ceramic multilayer systems.

4. Conclusions

The effects of residual stresses distribution on the interfacial adhesion energy of coatings were quantitatively investigated and related to the observed micro-mechanical behavior. The following conclusions could be drawn from this work:

1. An increase in average compressive residual stress in AlN coatings onto the silicon substrate was measured with an increase in bias-voltage and coating deposited with Al bond layer. Higher bias voltage accelerate the gas ions to the growing coating and additional energy caused the enhancement of residual stresses. It is also possible that the different bias conditions affect the interface between Si and AlN, in addition to increase the compressive residual stresses. The residual stress was further increased by adding an Al bond layer as a result of its high thermal expansion coefficient in comparison with AlN and silicon substrate. As a consequence, a tensile thermal stresses during cooling are established in Al which cause additional compressive residual stresses in AlN/Al coatings.
2. FIB-DIC residual stress depth profiles showed that (for the AlN/Al coatings) a strong residual stress gradient is present in the films, being the maximum compressive residual stress on the top surface, then decreasing towards the interface; a mild tensile stress is even observed for the AlN/Al-100V sample, which was the one showing more extended delaminations.
3. The coatings deposited without Al bond layer show significantly better adhesion in comparison with bond layer, even though both group of coatings have difference in compressive residual stresses equivalent to thermal stresses in bond layer. Adhesive failure could not be produced in coatings without a bond layer (AlN-30V and AlN-100V) even with cube-corner indenter, which means that interface adhesion is higher in comparison with coating deposited with Al bond layer. The fracture toughness corresponding to lateral cracks was measured to be 2.3 and 1.8 MPa $m^{0.5}$ for the coatings AlN-30V and AlN-100V, having residual stresses of 1.2 and 3.5 GPa, respectively. The observed behavior could be related to more homogenous compressive residual stress distribution in the AlN top-layer.
4. The adhesion energy for interface separation was found to be 5 and 4 J/m^2 for the coatings (AlN/Al-30V and AlN/Al-100V), having an average residual stresses of 1.5 and 3.9 GPa, respectively, with a corresponding interfacial fracture toughness of 0.71 and 0.65 MPa $m^{0.5}$, which is significantly lower than estimated fracture toughness of the AlN material, thus explaining why delamination occurs for AlN/Al systems. The tensile residual stress on the bond layer, coupled with its plastic deformation during indentation, leads to interface delamination.
5. These results suggested that in order to be beneficial for adhesion, a metallic bond layer should be with good hardness, small difference in thermal expansion coefficient and comparable elastic modulus with both the substrate and top-coating. Refractory metals being a good example for designing of improved multilayer coating systems with optimal performance.

Preprints (www.preprints.org) | NOT PEER-REVIEWED | Posted: 17 October 2018 doi:10.20944/preprints201810.0386.v1

Peer-reviewed version available at Nanomaterials 2018, 8, 896; doi:10.3390/nano8110896

Author Contributions: R. Ali and M. Renzelli performed the experimental activities and wrote most section of paper. M. Sebastiani, M. Imran Khan and E. Bemporad critically reviewed the experimental data and make the revisions in the paper.

Acknowledgments: The authors would like to thank Dr. Daniele de Felicis for his co-operation in focused ion beam imaging for coating thickness measurements. All the measurements and characterization activities were carried out at ''Inter-Departmental Laboratory of Electron Microscopy'' (LIME), University of ROMA TRE (http://www.lime.uniroma3.it), Italy.

Conflicts of Interest: The authors declare no conflict of interest.

References

1. Bian, Y., et al., Aluminum nitride thin film growth and applications for heat dissipation. Surface and Coatings Technology, 2015. 267: p. 65-69.
2. Abadias, G., et al., Stress in thin films and coatings: Current status, challenges, and prospects. Journal of Vacuum Science & Technology A: Vacuum, Surfaces, and Films, 2018. 36(2): p. 020801.
3. Ali, R., M. Sebastiani, and E. Bemporad, Influence of Ti–TiN multilayer PVD-coatings design on residual stresses and adhesion. Materials & Design, 2015. 75: p. 47-56.
4. Renzelli, M., et al., Design, fabrication and characterization of multilayer Cr-CrN thin coatings with tailored residual stress profiles. Materials & Design, 2016. 112: p. 162-171.
5. Kleinbichler, A., et al., New Insights into Nanoindentation-Based Adhesion Testing. JOM, 2017. 69(11): p. 2237-2245.
6. Kriese, M.D., W.W. Gerberich, and N.R. Moody, Quantitative adhesion measures of multilayer films: Part II. Indentation of W/Cu, W/W, Cr/W. Journal of Materials Research, 1999. 14(7): p. 3019-3026.
7. Khanna, V., Adhesion–delamination phenomena at the surfaces and interfaces in microelectronics and MEMS structures and packaged devices. Journal of Physics D: Applied Physics, 2010. 44(3): p. 034004.
8. Stoney, G.G., The tension of metallic films deposited by electrolysis. Proceedings of the Royal Society of London. Series A, Containing Papers of a Mathematical and Physical Character, 1909. 82(553): p. 172-175.
9. Janssen, G.C.A.M., et al., Celebrating the 100th anniversary of the Stoney equation for film stress: Developments from polycrystalline steel strips to single crystal silicon wafers. Thin Solid Films, 2009. 517(6): p. 1858-1867.
10. Advanced technical ceramics. Methods of test for ceramic coatings. Determination of internal stress by the Stoney formula, in BS DD CEN/TS 1071. 2005.
11. Daniel, R., et al., The origin of stresses in magnetron-sputtered thin films with zone T structures. Acta Materialia, 2010. 58(7): p. 2621-2633.
12. Korsunsky, A.M., M. Sebastiani, and E. Bemporad, Focused ion beam ring drilling for residual stress evaluation. Materials Letters, 2009. 63(22): p. 1961-1963.
13. Bemporad, E., et al., A critical comparison between XRD and FIB residual stressmeasurement techniques in thin films. THIN SOLID FILMS, 2014. 572: p. 224-231.
14. Korsunsky, A.M., et al., Nanoscale residual stress depth profiling by Focused Ion Beam milling and eigenstrain analysis. Materials & Design, 2018. 145: p. 55-64.
15. Oliver, W.C. and G.M. Pharr, An improved technique for determining hardness and elastic modulus using load and displacement sensing indentation experiments. Journal of Materials Research, 1992. 7(06): p. 1564-1583.
16. Toonder, J.D., et al., Fracture Toughness and Adhesion Energy of Sol-gel Coatings on Glass. Journal of Materials Research, 2002. 17(1): p. 224-233.
17. Thouless, M.D., An analysis of spalling in the microscratch test. Engineering Fracture Mechanics, 1998. 61(1): p. 75-81.
18. Castanho, J. and M. Vieira, Effect of ductile layers in mechanical behaviour of TiAlN thin coatings. Journal of Materials Processing Technology, 2003. 143: p. 352-357.
19. Chen, J. and S. Bull, Indentation Fracture and Toughness Assessment for Thin Optical Coatings on Glass. Vol. 40. 2007. 5401.
20. Pharr, G.M., W.C. Oliver, and D.S. Harding, New evidence for a pressure-induced phase transformation during the indentation of silicon. Journal of Materials Research, 1991. 6(6): p. 1129-1130.
21. Haberl, B., et al., Phase transformations induced in relaxed amorphous silicon by indentation at room temperature. Applied physics letters, 2004. 85(23): p. 5559-5561.

Preprints (www.preprints.org) | NOT PEER-REVIEWED | Posted: 17 October 2018 doi:10.20944/preprints201810.0386.v1

Peer-reviewed version available at Nanomaterials 2018, 8, 896; doi:10.3390/nano8110896

22. Liu, P., L. Cheng, and Y. Zhang, Measuring interface parameters and toughness—a computational study. Acta materialia, 2001. 49(5): p. 817-825.
23. Morris, D.J. and R.F. Cook, Indentation fracture of low-dielectric constant films: Part I. Experiments and observations. Journal of Materials Research, 2008. 23(9): p. 2429-2442.
24. Anstis, G., et al., A critical evaluation of indentation techniques for measuring fracture toughness: I, direct crack measurements. Journal of the American Ceramic Society, 1981. 64(9): p. 533-538.
25. Koumoulos, E.P., et al., Metrology and nano-mechanical tests for nano-manufacturing and nano-bio interface: Challenges & future perspectives. Materials & Design, 2018. 137: p. 446-462.
26. Bull, S.J., Nanoindentation of coatings. Journal of Physics D: Applied Physics, 2005. 38(24): p. R393 %@ 0022-3727.
27. Iriarte, G.F., et al., Influence of deposition parameters on the stress of magnetron sputter-deposited AlN thin films on Si (100) substrates. Journal of materials research, 2003. 18(2): p. 423-432.
28. Jones, A.M., et al., The effects of deposition temperature and interlayer thickness on the adhesion of ion-assisted titanium nitride films produced with yttrium metal interlayers. Nuclear Instruments and Methods in Physics Research Section B: Beam Interactions with Materials and Atoms, 1993. 80-81: p. 1397-1401.
29. Gerth, J. and U. Wiklund, The influence of metallic interlayers on the adhesion of PVD TiN coatings on high-speed steel. Wear, 2008. 264(9): p. 885-892.
30. Chen, J. and S. Bull, Approaches to investigate delamination and interfacial toughness in coated systems: an overview. Journal of Physics D: Applied Physics, 2010. 44(3): p. 034001.
31. Suo, Z. and J.W. Hutchinson, Interface crack between two elastic layers. International Journal of Fracture, 1990. 43(1): p. 1-18.
32. Ionescu, G., et al. Studies on Tribological Behavior of Aluminum Nitride-Coated Steel. in IOP Conference Series: Materials Science and Engineering. 2017: IOP Publishing.
33. Steinwandel, J., et al., Method and apparatus for aluminum nitride coating of a contact surface, especially a cylinder contact surface of a crankcase made of an aluminum basic alloy. 2001, Google Patents.
34. Pina Bhatt, D.H., Performance Evaluation of TiAlN and CrN Coated Silicon Wafer by Magnetron Sputtering Method. International Journal of Nanotechnology and Applications, 2017. 11(2): p. 167-177.